INT. J. REMOTE SENSING, 20 NOVEMBER, 2004,
VOL. 25, NO. 22, 5131–5141

An approach for correcting inhomogeneous atmospheric effects in remote sensing images

M. HASHIM

Faculty of Geoinformation Science & Engineering, Universiti Teknologi Malaysia, Locked Bag 791, 80990 Johor Bahru, Malaysia;
e-mail: mazlan@fksg.utm.my

A. WATSON and M. THOMAS

Department of Environmental Sciences, University of Stirling, Stirling FK9 4LA, UK

(*Received 11 October 1996; in final form 9 February 2004*)

Abstract. Two contextual-based approaches for correcting first order atmospheric effects due to atmospheric inhomogeneity and adjacency effect are described. The first method is a modification of the restoration method for the adjacency effect suggested by Richter. The second method is an adaptation of Stenberg's rolling ball algorithm using the mathematical morphology transformation. Evaluation of the proposed method was carried out by noting classification accuracy on the basis that an increase in classification accuracy reflects in improved image quality. Results show that the average accuracy of classification of a scene from Malaysia, with 13 ground truth classes was as follows: (a) uncorrected—86%, (b) adjacency correction—86%, and (c) rolling ball correction—89%. It is clear from the results that the rolling ball method of correction does yield an increase in accuracy although not as substantial as in this case, and there is no reason to doubt that this method could be used to correct a wide variety of images that are affected by inhomogeneity of the atmosphere.

1. Introduction

Success in extracting land surface information using satellite remotely sensed data relies heavily on the spectral data quality of the imagery. Unfortunately, in many instances the quality of the image is influenced by the atmospheric conditions during the data acquisition. The atmospheric effects are dependent on the type of surface, atmospheric optical properties (aerosol thickness, visibility), and wavelength used in the recording of the data (Duggin 1985). Due to the atmospheric effect, especially for imagery recorded in the shorter wavelengths (visible to near infrared), where more vigorous molecular and aerosol scatterings take place, the differences between spectral reflectance from different surfaces are difficult to discriminate and this leads to a decrease in the accuracy of the surface classification (Kaufman and Fraser 1984, Kaufman 1985).

Numerous studies have been conducted with different approaches to the

International Journal of Remote Sensing
ISSN 0143-1161 print/ISSN 1366-5901 online
http://www.tandf.co.uk/journals
DOI: 10.1080/01431160410001712971

problems of minimizing the atmospheric effects in satellite remotely sensed data. In general, the existing atmospheric correction methods treat the atmosphere as homogeneous over the entire scene. This, however, is rarely realistic. The atmosphere in fact, varies spatially and the variation can usually be seen on any display system. In addition to the existence of inhomogeneity of atmospheric effect, there also exists a scattering effect due to the reflection of upward radiation coming from neighbouring pixels particularly in scenes with small heterogeneous irregular-surfaced fields. This later atmospheric effect is known as the adjacency effect, which tends to broaden the signature probability distribution of spectral classes, hence causing lower separabilities of classes (Kaufman 1989). Most of the current methods of atmospheric correction ignore this effect. This paper introduces two new approaches to minimize atmospheric effects, neither of which make any assumption about the atmosphere nor require input from corresponding *in situ* atmospheric data. Both approaches provide a relatively simple way of correcting atmospheric effects using contextual information. The first method is a modification of the restoration method for the adjacency effect suggested by Richter (1990). The second method is an adaptation of Stenberg's (1986) rolling ball transformation.

2. New approach for minimizing atmospheric effects

Two new techniques for minimizing atmospheric effects are introduced based on the fact that the atmosphere is not homogeneous over the scene. In this new approach, the atmosphere is treated as a horizontal continuum dependent on atmospheric turbidities rather than as being horizontally stratified, and minimization of atmospheric effects, therefore, can be carried out in a contextual approach. In essence, atmospheric correction with a contextual approach treats the multiple scatterings (upward radiances of a heterogeneous field with non-uniform surfaces) as local variations, while the path radiances are treated as gross variations in the background intensities. This is approximated by Richter (1990) as:

$$\rho^{(2)} = \rho^{(1)} + q\left[\rho^{(1)} - \rho'^{(1)}\right] \tag{1}$$

where $\rho^{(2)}$ is the final surface reflectance, $\rho^{(1)}$ is the surface reflectance,

$$q = \int_{\lambda_1}^{\lambda_2} \frac{\tau_{dif}}{\tau_{dir}} \phi(\lambda) \mathrm{d}\lambda \tag{2}$$

$$\rho'^{(1)} = \frac{1}{N} \sum_{j=1}^{N^2} \rho_j^i \tag{3}$$

N is the average reflectance defined locally within a specific odd-size window, and the central pixels are considered in every computation, $\frac{\tau_{dif}}{\tau_{dir}}$ are direct and diffuse transmittance (ground to sensor), respectively; and λ_1, λ_2 are the minimum and maximum wavelengths of a band.

Having said these two variations (local variations of the multiple scatterings and gross variations in the background intensities) existed in the image, the contextual methods were tested to reduce these variations. The basic idea of how this operation is carried out rests on the fact that a scene affected by atmospheric effects is made up of several homogeneous atmospheric regions which could contain

variable degrees of atmospheric effects. In the contextual approach, the region can be adequately defined by a window.

2.1. *Method 1—Inhomogeneous atmospheric effect correction*

The correction is performed by subtracting variations due to the inhomogeneous atmosphere from its original raw data. Each of the spectral band's data are corrected independently. By implementing this method the following series of image processing opeations is carried out: (i) creation of local minimum templates, (ii) estimation of background errors due to path radiance and removal of local variations due to multiple scatterings producing smoothed local minimum, and (iii) removal of background errors.

In step (i) the raw input image of Landsat TM is partitioned into a 32×32 pixel window, representing variations in area of approximately 10×10 km. Using this window, the study area of 1024×1024 is partitioned into 32×32 pixel templates, respectively. The window size is invariable, and a 32×32 pixel window is chosen in this study to represent the significance of atmospheric variations to the nearest kilometre. As suggested by Richter (1990) the selection of window size depends on various factors which include the pixel size, spectral and spatial frequencies of the scene, and also atmospheric parameters. Various window sizes ranging from 7–35 pixels have been tested in this study, and 32×32 pixel windows are found best representing the so-called atmospheric region other than partitioning the input raw image into the exact number of templates.

In step (ii) the minimal value of the raw data for every template is determined. These minimum grey level values represent the background errors due to path radiance. Kaufman (1989) found that dark surfaces (areas with minimal grey level values) are most affected by atmospheric scattering, therefore ensuring these surfaces can be used adequately to estimate the path radiance. The minimal template is then smoothed. This procedure is to ensure continuity of the estimated background error within a region that can be smoothly matched to the adjoining regions, which eventually forms a continuous estimated background error for the entire input scene. Smoothing is carried out using the rolling ball transformation (Stenberg 1986). Also within this transformation, the local variations in the background errors are minimized.

In the rolling ball transformation (RBT) process, the image is viewed as a set of boxels or umbra (cubical pixels) in 3-dimensional space (see figure 1). The pixel and row number form the umbra abscissa and ordinate while the pixel intensity is the height of the boxel. The ball is moved freely on the umbra. The centre of the ball is determined by finding the maxima and then minima values within the umbra of the minima-template. The trajectory of the ball's centre is the smoothed image. The transformation process is then repeated with the ball placed below the umbra surface for picking up the dimples; this process is known as opening. The same transformation process, with the ball gliding on the umbra is called closing.

Opening and closing are two terms in mathematical morphology referring to image transformation which employ structural elements as operators to transform the input pixel of an image according to the relationship of each pixel to other pixels within the neighbourhood. The structural element in the RBT is a sphere

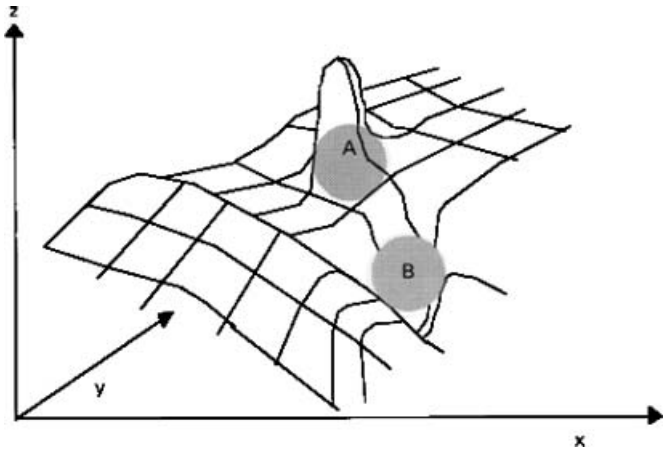

Figure 1. Schematic representation of the rolling ball transformation. The image from each spectral band is viewed as boxels. In the transformation process, the opening glides the ball onto the umbro, and closing glides the ball under the umbra following the background contours but does not penetrate the spike A or dimple B (modified from Stenberg 1986).

(ball). An opening of an image X by structuring element Y is given by:

$$X_Y = [X \Theta Y] \oplus Y \tag{4}$$

and likewise, closing is given by:

$$X_Y = [X \oplus Y] \Theta \mathrm{Y} \tag{5}$$

where $\oplus$ is the Minkowski addition, which is determined by translating Y by each element of X and then taking the union of all the resulting translations; and Θ is the Minkowski subtraction determined by translating every element of Y by each element of X and then taking the intersection of all the resulting translations.

The complete RBT process generates two resultant images: (a) a smooth image with both spikes and dimples removed, and (b) a rough image, a combination of spikes and dimples. As the interest of this paper is the removal of variations due to atmospheric effects, only the smoothed image is important. This is a smoothed local minimum image.

In step (iii) two operations are performed. First, the smoothed local minimum is expanded back to its original input size. This is achieved by interpolating the minimum value of the raw image using the smooth local minimum template. The cubic b-spline interpolation method uses 16 neighbouring points from the raw data. The product of the interpolation is an expanded (full size) transformed minimum. Second, this interpolated minimum is then subtracted from the original image to give the final background-normalized image, free from the effect of backscatter.

2.2. *Method 2—Adjacency effect correction*

This correction is based on the assumption that re-scattering of the upward radiance can be adequately minimized by a convolution filter. Given the known fact that the de-blurring effects can generally be sharpened using convolution filters (Mather 1987, Geman and Geman 1984), a replicate of the resultant effects can then be taken into account in the correction of the affected images. The adjacency

effect blurs the pixel of interest (apparent IFOV) due to the radiance of neighbouring reflections (intrinsic IFOV). As in a general linear system, the radiance response of the IFOV is normally given as a point spread function (PSF), and the intrinsic IFOV in this case is a minor PSF occurring within the previous major PSF. The notion of this effect and the previous factors are then adapted in the correction filter. The correction filter works as in the low pass convolution filtering where the central pixel is replaced by the resultant neighbourhood measure used in the filtering. In this study, the filter kernel set is a weighted gaussian scattering function occurring in a specific window size. Richter (1990) used a similar concept to minimize the adjacency effect but an average square filter is used instead.

In generating the filter kernels, the gaussian scattering function estimates the scattering due to adjacency effects as symmetrically distributed around the central pixel. This is used to assimilate the PSF of the radiance response within a detector against the background radiance. As such, the central pixel of a specified window experiences the most adjacency effect, and the effect decreases with distance from the central pixel. The scattering effects due to the adjacency variations must however, ensure that the filtering only enhances the affected details without changing the image background information. The weights in the filter kernels are determined by an exponential function, with the central pixel having the maxima peak and the adjacent pixels taking a value determined by the exponential function with respect to distance from the central pixel. Examples of the gaussian-based kernel filters for 5×5, and 7×7 windows are given in figure 2.

The filter size is set to a reasonable size so as to represent the adjacency effect. It is also representative of the local contrast. In the study area, where field sizes vary from small holdings up to large estate holdings, windows of 3×3, 7×7, 11×11, 15×15 and 25×25 were then tested. In selecting the window sizes for the possibilities of minimizing the adjacency effect, the scattering radius must also be considered. The relationship of the scattering radius and the filtering window is given as $2L+1$ pixels, where L is the scattering radius. If the filter size that reasonably represents the object of interest is 3×3, then the scattering radius is 1 (in pixel units). The correction procedures are performed as follows:

(i) Generate the filter kernel set by using the gaussian function for the selected window size. The central weights are set to zero.
(ii) Filtering using the convolution approach where the filter kernel acts as the mask in the process.
(iii) Using the filtered image as an input, the initial kernel set is refined. This is carried out by first creating a suitable histogram range that can adequately represent the image information content. Within this range, introduce the scattering effect in an iterative manner, where in each pass a fractional scattering value of 0.1 is increased, until the number of zero bins in the histogram is at a minimum. The initial value of scattering is set to 0.1; the minimum adjacency effect proposed by Richter (1990).

A test was conducted to identify the most effective window size for this filtering process. Summarizing the test only on Lansat Thematic Mapper (TM) band 1, results presented in table 1 show that the filter is able to remove the unwanted noise, while preserving the fidelity of the background information. This is clearly shown by the image statistical properties. This, however, is only valid for a window size in the range of 3×3 to 15×15. Larger windows tend to over-correct the smearing,

$57x10^{-4}$	$3.15x10^{-3}$	$8.55x10^{-3}$	$3.15x10^{-3}$	$57x10^{-4}$
$3.15x10^{-3}$	$6.32x10^{-2}$	0.172	$6.32x10^{-2}$	$3.15x10^{-3}$
$8.55x10^{-3}$	0.172	0	0.172	$8.55x10^{-3}$
$3.15x10^{-3}$	$6.32x10^{-2}$	0.172	$6.32x10^{-2}$	$3.15x10^{-3}$
$1.57x10^{-4}$	$3.15x10^{-3}$	$8.55x10^{-3}$	$3.15x10^{-3}$	$1.57x10^{-4}$

$5.54x10^{-5}$	$5.11x10^{-4}$	$1.94x10^{-3}$	$302x10^{-3}$	$1.94x10^{-3}$	$5.11x10^{-4}$	$5.54x10^{-5}$
$5.11x10^{-4}$	$4.7x10^{-3}$	$1.79x10^{-4}$	$2.79x10^{-2}$	$1.79x10^{-4}$	$4.7x10^{-3}$	$5.11x10^{-4}$
$1.94x10^{-3}$	$1.79x10^{-2}$	$6.78x10^{-2}$	9.106	$6.78x10^{-2}$	$1.79x10^{-2}$	$1.94x10^{-3}$
$3.02x10^{-3}$	$2.79x10^{-2}$	$6.78x10^{-2}$	0.106	$6.78x10^{-2}$	$1.79x10^{-2}$	$1.94x10^{-3}$
$1.94x10^{-3}$	$1.79x10^{-2}$	$6.78x10^{-2}$	0.106	$6.78x10^{-2}$	$1.79x10^{-2}$	$1.94x10^{-3}$
$5.11x10^{-4}$	$4.71x10^{-3}$	$1.79x10^{-4}$	$2.79x10^{-2}$	$1.79x10^{-4}$	$4.71x10^{-3}$	$5.11x10^{-4}$
$5.54x10^{-5}$	$5.11x10^{-4}$	$1.94x10^{-3}$	$3.02x10^{-3}$	$1.94x10^{-3}$	$5.11x10^{-4}$	$5.54x10^{-5}$

Figure 2. Example of the 5×5 and 7×7 gaussian-weighted kernels used for smoothing.

thus producing an image with linear features more depictable but broadened the overall image contrast.

3. Evaluation

Evaluation of the two atmospheric correction methods was determined by noting the classification accuracy on the basis that an increase in classification

Table 1. The image statistical properties before and after being treated with the adjacency correction.

	Filter parameters*			Image parameter					
Feature	Window	Scat radius	Scat	Minima	Maxima	Mean	Median	Mode	Standard deviation
Band 1	Untreated	Untreated	Untreated	49	255	67.090	64	62	11.456
	3×3	1	0.1	36	255	67.099	64	62	12.542
	7×7	3	0.1	0	255	67.031	64	61	19.169
	11×11	5	0.1	14	255	67.082	64	61	13.834
	15×15	7	0.1	18	255	67.075	64-	61	14.391
	25×25	12	0.1	0	255	66.930	63	58	22.700

*Note: Scat radius = scattering radius, and Scat is the minimal increment adjacency effect.

accuracy reflects an improvement in the image quality. The classification accuracy is determined by the contigency matrix and the overall performance of classification by the Kappa coefficient of agreement (Hudson and Ramn 1987) of the classified image using data treated with the appropriate correction methods. Apart from these two contextual approaches, a widely used first-order atmospheric correction—the improved dark subtraction method (Chavez 1988) is also used as a comparison. In this method the correction is carried out by subtracting the haze values for all respective spectral band data using a relative atmospheric scattering model to predict the haze values of a selected starting haze value from a particular band dataset.

3.1. *Test site*

A Landsat-5 TM 1024×1024 subscene of path/row 128/57, covering an approximate area of $625\,km^2$ situated on the western coastline of Malaysia was used in the application test. The area has a good representation of mixed land cover types ranging from actively cultivated agricultural lands, urbanized areas, various ranges of forested lowlands and uplands to freshwater and mangrove swamps. The categories extracted from the present land use map of the corresponding area are used to label the spectral groups formed by the classifiers, while independent test sets are randomly selected from the classified, labelled image. The test polygons were identified on satellite imagery, verified in the field before the accuracy assessments are made.

3.2. *Image classification*

Two classifiers were used in the classification of the atmospherically corrected image: (i) the combined unsupervised/supervised maximum likelihood (CMLH) and (ii) the 2-dimensional watershed method (Watson *et al*. 1992). The CMLH involves two steps starting with clustering the image into an initial 100 spectral classes, which are then used as training seed in the following maximum likelihood classification. Both the non-parametric approach classifications are purposely chosen to counter in the best possible way any non-linearity of spectral data due to the proposed correction.

4. Results and discussion

The results of the classifications are summarized in table 2. The overall accuracies of the classified image using the improved dark subtraction method are the same as when the untreated data were used in the classifications. This result is as might be expected, as the linear shift within the spectral band only affects the global dynamic shift in all the images, but does not change the internal structure of the spectral signatures within the feature spaces. In other humid tropical land cover studies, similar atmospheric corrections (dark methods), where linear shifts were used in the spectral data for compensating the atmospheric effects, do not significantly affect the signatures of feature classes (Etchegory and Gambart 1991).

Using the treated data for inhomogenous atmospheric correction (method 1), the overall class accuracy was improved in the study area. With the watershed classification, correcting the inhomogeneity backscatter reduced the omission and commission errors. This is indicated by the increase in kappa coefficient from 0.848 to 0.885. This is again evident by the increase in the kappa coefficient in the CMLH classification from 0.612 to 0.678. The variations removed are minimal, therefore

Table 2. Overall average classification accuracy and kappa coefficient of agreement (κ) with features pre-corrected for atmospheric effects using method 1—inhomogeneity of backscattering, method 2—adjacency, and its comparison with features corrected with method 3—improved dark subtraction technique (Chavez 1988). L_c denotes scattering radius, which determines the corresponding window size as $2*L_c+1$.

		Per cent classified into class														
Classifier	Treatments	1u	lt	2h	3c	3g	3o	4c	4p	6	7f	7s	7c	8	Average	κ
CMLH	Untreated	39	61	62	61	55	31	54	0	45	94	77	35	86	58	0.612
	Method 1	55	85	85	84	78	44	76	37	63	94	83	49	8	71	0.678
	Method 2 (L_c2)	36	41	60	39	66	33	42	0	39	0	77	0	82	42	0.481
	Method 2 (L_c3)	41	63	63	46	52	50	39	0	44	63	75	0	85	49	0.564
	Method 2 (L_c5)	37	78	98	85	93	48	42	44	60	10	95	21	98	62	0.734
	Dark Method	39	61	62	61	58	31	54	0	45	94	77	35	89	58	0.614
Watershed	Untreated	86	76	83	85	83	100	89	85	86	76	91	85	91	86	0.848
	Method 1	84	85	83	84	90	88	88	90	83	93	92	95	97	89	0.885
	Method 2 (L_c2)	47	62	52	69	87	45	81	32	54	69	81	54	92	63	0.692
	Method 2 (L_c3)	49	68	64	70	83	50	86	34	65	60	88	33	95	65	0.719
	Method 2 (L_c5)	85	74	83	85	100	83	89	85	86	75	91	85	92	86	0.860
	Dark Method	86	76	83	85	83	100	89	85	86	76	91	85	91	86	0.848

1u, urban and associated areas; 1t, tin mining areas; 2h, horticulture; 3c, coconut; 3g, rubber; 3o, oil palm; 4c, diversified crops; 6, grassland; 7f, forest; 7s, scrubs; 7s, cleared lands; and 8, swamps and wetlands.

the resultant spectral band corrected by this technique also contains a rather smooth surface which requires rather sensitive classifiers to differentiate the spectral groups. This is exhibited more by the watershed method compared to the maximum likelihood classification.

Feature inputs treated for adjacency correction (method 2) exhibit variable results in the final classification accuracies depending on the window sizes. In the tested window sizes of 5, 7, and 11 pixels, adjacency corrections show that they are more discriminatory in the larger windows. This is shown in all the tests that small window smoothing using a gaussian-kernal filter tends to over-correct the effect of adjacency. Window size up to 5×5 pixels has a negative impact on the classification accuracies. Visually, however, the smaller filter 5×5 is able to suppress bright spots within bright areas or even suppress dark spots from the less dark surroundings. In terms of removing local variations and enhancing the local contrast, window size 11×11 shows the best result. Overall average accuracy does not change significantly, but the errors of commission and omission are reduced, as shown by the increase in the kappa values. The minimal improvement in the classification accuracy, however, is in accordance with previous works such as those of Gonima (1993) where adjacency effect magnitude is in the range of 0.5–12%.

The adjacency effects are seen to be closely dependent on the window sizes. Given the study area characteristics, the land use classes are more generally better discriminated with a window larger than 5×5 pixels. The only drawback is that the larger window sharpens the edges and spatial variation; hence the overall image

characteristics are not altered but increase the information content as a result of the larger contrast produced. The best classification accuracy result is given by the features corrected with method 1—the inhomogeneous atmospheric correction, classified with the watershed method (figure 3).

5. Conclusion

In this paper, two contextual-based atmospheric correction approaches for minimizing the backscattering effects of an inhomogeneous atmosphere and adjacency effects due to heterogeneous irregular-shaped fields have been described. Method 1 smoothed the atmospheric inhomegeneity variations by adapting the rolling ball algorithm, while method 2 calculated the local variations due to the adjacency effect by using a gaussian-function convolution filter.

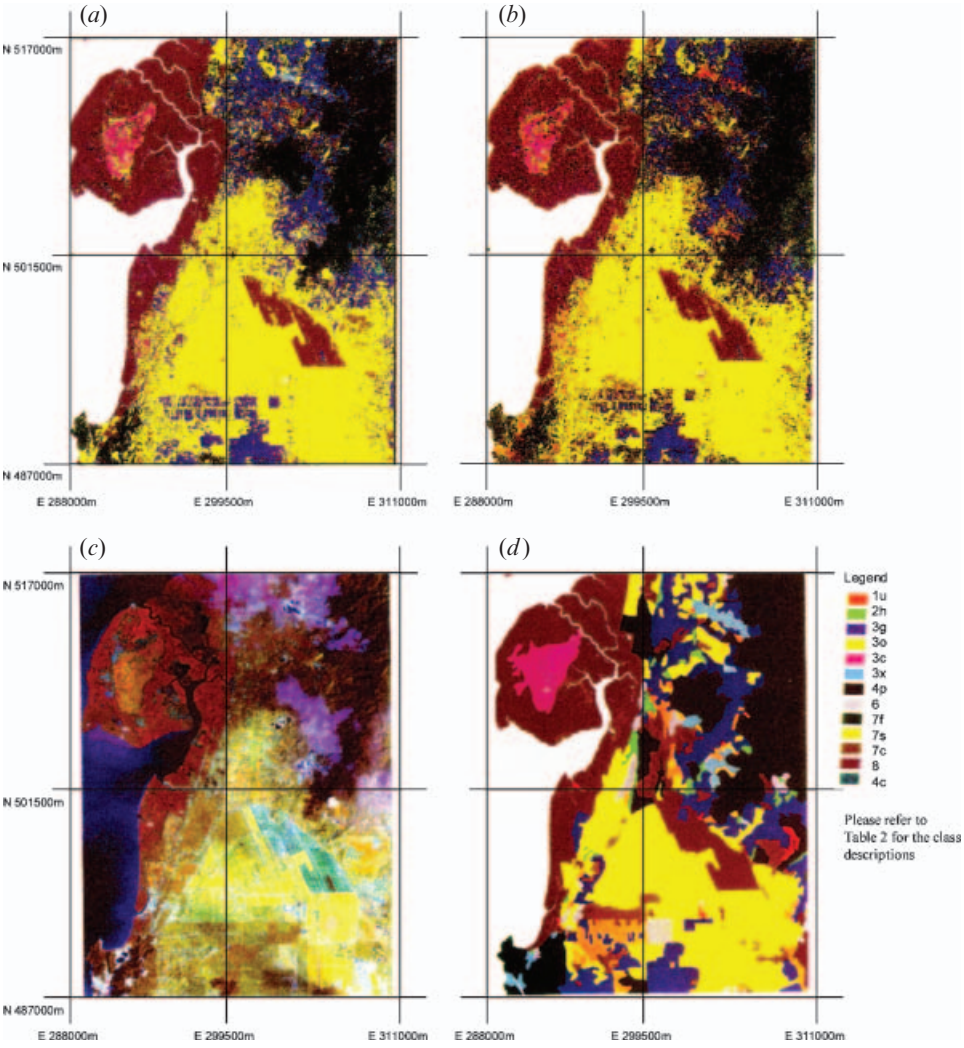

Figure 3. Final classified image using (*a*) untreated spectral bands; and (*b*) spectral bands treated for atmospheric inhomogeneity (method 1); (*c*) the image (note the inhomogeneous haze), and (*d*) corresponding land use classes.

The classification accuracies of Landsat TM data treated with these approaches were assessed with image data acquired from both study areas. The land use categories or classes obtained from the present land use map were used in the analysis. Results showed that method 1 is able to minimize local atmospheric variations and can reduce spectral confusions by up to 38% (0.135 in terms of kappa coefficient difference). Similarly, the adjacency effects are seen to be closely dependent on the window sizes. Given the study area characteristics, the land use classes are more generally better discriminated with a window larger than 5×5 pixels. The only drawback is that the larger window sharpens the edges and spatial variation; hence the overall image characteristics are not altered but increase the information content as a result of the larger contrast produced. The best classification accuracy result is given by the features corrected with method 1—the inhomogeneous atmospheric correction, classified with the watershed method (figure 3). Method 2 also demonstrates the ability to minimize the local variations due to the adjacency effect if the right relationship of object-to-window size is understood. The image corrected with method 2 reported a consistently better classification result than the linear shift method as used in most general haze corrections (Chavez 1988, 1992).

As operational classification accuracies (in excess of 90%) are still hardly met by most remote sensing users (Townshend 1992), these two new approaches have shown potential pre-processing tasks for the removal of unwanted atmospherical variations in order to produce a more accurate image classification. Results demonstrated in this paper suggest strongly that these techniques can be used to remove local atmospheric effect variations. Although the atmospherically-based variations proved not to provide a major means of making an accurate digital classification, their correction has been proved to lessen the confusion among spectral signatures within the spectral data. Similar results obtained by Hashim (1995) also confirmed that atmospherically corrected images contained less confusion and omission errors. Other than these variations that restrict optimal classification accuracy, the inherent spatial and background regional information could also have possible close influences.

References

CHAVEZ, P. S. JR., 1988, An improved dark-object subtraction technique for the atmospheric scattering correction of multispectral data. *Remote Sensing of Environment*, **24**, 459–479.

CHAVEZ, P. S. JR., 1992, Comparison of spatial variability of visible and near-infrared spectral images. *Photogrammetric Engineering and Remote Sensing*, **58**, 957–964.

DUGGIN, M. J., 1985, Factors influencing the discrimination and quantification of terrestrial features using remotely-sensed radiance. *International Journal of Remote Sensing*, **6**, 3–27.

ETCHEGORY, G., and GAMBART, D. D., 1991, Computer-assisted land cover mapping with SPOT in Indonesia. *International Journal of Remote Sensing*, **12**, 1493–1507.

GEMAN, S., and GEMAN, D., 1984, Stochastic Relaxation, Gibbs Distributions, and the Bayesian restoration of images. *Visual System Architectures IEEE Transactions on Pattern Analysis and Machine Intelligence*, **6**, 721–741.

GONIMA, L., 1993, Simple algorithm for the atmospheric correction for reflectance image. *International Journal of Remote Sensing*, **14**, 1179–1187.

HASHIM, M., 1995, Classification of Landsat Thematic Mapper Data for Land Cover Mapping in Malaysia: a morphological and contextual approach. PhD Dissertation, University of Stirling, UK, 400 pp.

HUDSON, W. D., and RAMN, C. W., 1987, Correct formulation of kappa coefficient of agreement. *Photogrammetric Engineering and Remote Sensing*, **53**, 421–422.

KAUFMAN, Y. J., 1989, The atmospheric effect on remote sensing and its correction. In *Theory and Applications of Optical Remote Sensing*, edited by G. Asrar (New York: John Wiley), pp. 337–428.

KAUFMAN, Y. J., 1985, The atmospheric effect on the separability of field classes from satellites. *Remote Sensing of Environment*, **18**, 21–34.

KAUFMAN, Y. J., and FRASER, R. S., 1984, The atmospheric effect on the classification of finite fields. *Remote Sensing of Environment*, **15**, 95–118.

MATHER, P. M., 1987, *Computer Processing of Remotely-sensed Images*: *An Introduction* (Chichester: John Wiley).

RICHTER, R., 1990, A fast atmospheric correction algorithm applied to Landsat TM images. *International Journal of Remote Sensing*, **11**, 159–166.

STENBERG, S., 1986, Greyscale morphlogy. *Computer Vision, Graphics, and Image Processing*, **35**, 333–355.

TOWNSHEND, J. R. G., 1992, Land cover: in search for applications. *International Journal of Remote Sensing*, **13**, 1319–1334.

WATSON, A. I., VAUGHAN, R. A., and POWELL, M., 1992, Classification using the watershed method. *International Journal of Remote Sensing*, **13**, 1881–1890.